energies

MDPI

Article

Holistic Approach for an Energy-Flexible Operation of a Machine Tool with Cooling Supply

Martin Lindner *, Benedikt Grosch, Ghada Elserafi, Bastian Dietrich and Matthias Weigold

Institute of Production Management, Technology and Machine Tools (PTW), Technical University of Darmstadt, Otto-Berndt-Str. 2, 64287 Darmstadt, Germany; b.grosch@ptw.tu-darmstadt.de (B.G.); g.elserafi@ptw.tu-darmstadt.de (G.E.); b.dietrich@ptw.tu-darmstadt.de (B.D.); m.weigold@ptw.tu-darmstadt.de (M.W.)

* Correspondence: m.lindner@ptw.tu-darmstadt.de

Abstract: The following paper examines the practicality of a methodical approach for energy-flexible and energy-optimal operation in the field of metal-cutting production. The analysis is based on the example of a grinding machine and its central cooling-supply system. In the first step, an energy-flexibility data model is built for each subsystem, which describes energy flexibility potentials generically. This is then extended to enable combined energy cost-optimal production planning. As a basis for the links between the data model representations, the cold flows between the subsystems are modeled using parameter-estimation methods, which have a mean absolute error of only 2.3 percent, making the subsequent installation of heat meters unnecessary. Based on the presented approach, the results successfully validate the possibility of energy-flexible cost-optimal and sensor-reduced production planning by reducing energy costs by 6.6 percent overall and 1.9 percent per workpiece produced.

Keywords: energy flexibility; manufacturing; machine tool; optimization; demand-side management

1. Introduction

The increase in volatile renewable energy sources in combination with the continuous reduction in fossil power plants are reasons for growing fluctuations in power grids, for instance, in Germany [1]. These fluctuations of electricity generation are mainly caused by changing weather conditions affecting wind and solar power [2].

Demand response (DR) involves measures for adjusting power consumption profiles according to energy price signals or providing energy flexibility capacity to help maintain power grid stability. Along with actions related to energy efficiency, DR could be a promising tool for tackling the challenges of fluctuating power supply [3]. Both DR and energy efficiency constitute demand-side-management (DSM) activities that aim to adjust the amount and/or timing of electricity consumption [4].

For this reason, the German research project "SynErgie" [1] focuses on the DSM of industrial processes, which accounts for 44 percent of gross energy consumption in Germany [5]. One of the main results of the last five years of research is a generic energy flexibility data model (EFDM) for describing energy flexibility potentials with respect to the power consumption of machines and systems in the industrial sector [6]. This model uses standardized description and key figures for modeling power-related energy flexibility. However, the data model has not been applied to real industrial use cases so far. In this context, this paper examines the practical usability of this approach for assessing energy flexibility potentials in the field of machining.

DR as such is already carried out by some of the biggest energy consumers of the German industry such as the production of basic metals, paper and paper products, and chemicals and chemical products. Electricity-intensive production processes involved in these industries offer large amounts of flexibilizable power by means of load reduction and load shifting [7]. The marketing of energy flexibility on balancing energy or spot markets

check for updates

Citation: Lindner, M.; Grosch, B.; Elserafi, G.; Dietrich, B.; Weigold, M. Holistic Approach for an Energy-Flexible Operation of a Machine Tool with Cooling Supply. *Energies* **2023**, *16*, 3943. https://doi.org/10.3390/en16093943

Received: 17 April 2023
Revised: 2 May 2023
Accepted: 4 May 2023
Published: 7 May 2023

could be profitable for industrial companies, which would create incentives for more energy flexibility to be provided [8]. Transparency and support mechanisms regarding energy flexibility in industrial settings should therefore be promoted and utilized. As Sauer et al. point out, energy flexibility is already used economically in energy-intensive industries. Similarly, Sauer et al. also show that small consumers, as a whole, have a large flexibility potential [1]. However, this potential is not being realized since individual small flexibilities are not economically useful for large-scale electricity markets. The above-mentioned data model could be a useful tool to capture and aggregate small flexibilities in a standardized way so that they can be treated as one large flexibility and traded in respective market places.

1.1. Related Work

Further, Bank et al. [3] show that it is fundamentally possible to implement energy flexibility based on a data model with energy-oriented production planning. This presents the possibility to participate more effectively in energy markets. However, the supply systems of the considered loads are not taken into account. Furthermore, the optimization of the machines shown in Bank et al. is only based on the underlying energy price curve and does not take into account the available energy in the supply systems. Seitz et al. [9], on the other hand, show an approach that fundamentally allows several levels, e.g., production machines and supply technology, to be considered together in an energy-flexible optimization. However, the approach has not yet been applied. Roth et al. [10] consider the supply system in the energy-flexible PPS in which a battery storage is taken into account. However, no uniform data model is used in his work. Kehne et al. [11] show that for the energy-flexible operation of a machine tool, the optimization of the process itself is also possible. In this approach, however, the machine operation is also carried out only according to volatile energy prices without taking into account the supply technology of the plant. In addition, Popp et al. [12] shows that an optimized machine tool operation can also be carried out under the consideration of dependencies. For this, Popp considers the components of the machine tool but not the supply systems or production specific dependencies of the plant. Additionally, a standardized data model is not used, which makes it a use-case-specific solution. In contrast, Bahmani et al. [13] show that energy-flexible production planning based on a generic data model and taking dependencies into account is possible. However, its functionality is only shown in synthetic use cases.

1.2. Research Gap

The following work aims to address obstacles in realizing energy flexibility potential in the field of machining, which is considered a small consumer, by demonstrating the feasibility of using a standardized data model for flexibilizing processes with small individual electrical consumption but notable collective flexibility potential. The presented use case involves a modern computer numerical control (CNC) grinding machine tool with its corresponding workpiece storage and central cooling supply, which represents a realistic but simple manufacturing setting. In addition to exhibiting the practicality of the aforementioned EFDM based on [6], this work establishes an approach for including energy flexibility considerations in production planning while keeping the model compatible with energy-market-specific requirements and conditions. In the practical application of the data model, several obstacles arise. These and open points of previous related works are addressed in our paper. The following aspects outline the contribution of our work:

- Most of the previous related work does not calculate a (detailed) EFDM with consideration of the production plan. We propose an approach to achieve both an energy-flexible production plan and a detailed EFDM. Therefore, we take into account the material flow of the machine tool while calculating the EFDM and the optimization of the production plan.

- Previous research does not address a machine tool in combination with its energy-supply systems. Those systems under consideration are usually highly dependent on each other and can therefore not be modeled in disjoint data models. In our presented use case, the cooling-supply system has to provide enough cooling capacity for the operation of the machine tool. So, we take both systems into account while modeling the EFDMs with their dependencies.
- Our presented approach shows which assumptions and simplifications are needed to fill out the data model and parameterize the resulting optimization problem.

The above points close the gap between the theory, modeling, and application of energy flexibility in a real production environment. The shown approach is transferable to other use cases, e.g., from the paper industry and other storage systems. This is made possible by the generic data model used and the solution shown for optimization with the necessary calculations. These address the research question of how the key figures of the EFDM can be calculated for a real use case and which data are necessary for energy-flexible optimization. The remainder of this paper is organized as follows. In Section 2, basic theoretical insights about the structure of the EFDM and production scheduling are given. Similarly, the section briefly shows the basics of virtual metering in combination with the parameter estimation of volume flow. The experimental use case is explained in Section 3. For the calculation of the EFDMs, the cold flows between the cooling-supply system and the grinding machine are needed, which have to be measured by sensors. Since, in practice, sensors cannot be installed everywhere, a virtual sensor is developed and modeled to estimate the cold flows in Section 4. In Section 5, we initially establish a specific EFDM for each component of the use-case based on equations or manufacturers' specifications. Therefore, the creation of specific EFDMs of the machines is described, which are used in the experimental system setup. In Section 6, the experimental application and the results of the energy-flexible operation are described. The energy-flexibility measures involved in the optimized energy-flexible load profile are subsequently applied to the use-case during the practical operation of the components, followed by evaluation and discussion. Finally, Section 7 gives a conclusion of the results and provides approaches for further research.

2. Theoretical Background

Our research is based on the methodology presented in [6], which aims to describe possible energy flexibilities of physical systems using generic EFDM. As shown in Figure 1, the three classes *Flexible Load*, *Flexible Storage*, and *Dependencies* of the EFDM span the *Flexibility Space*. This space contains all of the possibilities of an energy-flexible system to vary its energy output compared to the reference case.

Therefore, a method for representing a production system using EFDM is demonstrated, and the respective boundary conditions necessary are presented. On this basis, the energy demand of the production machine and the associated supply systems is examined under the consideration of estimated thermal energy flows using virtual flow sensors. This offers the advantage that no complex and costly sensor retrofitting is required and is explained in-depth in Section 2.3.

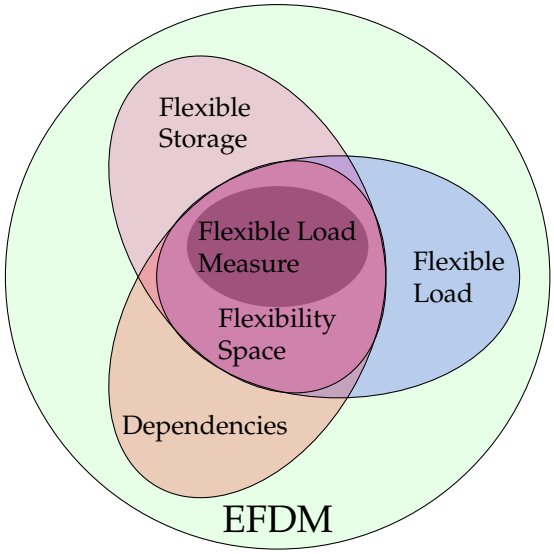

Figure 1. The Figure shows the three different classes of the energy flexibility data model (EFDM), which create the *Flexibility Space*, which contains the class of possible *Flexibility Load Measures*.

2.1. Energy-Flexibility Data Model

In the following, we give a description of the energy flexibility data model (EFDM) classes. These general descriptions are provided in [6], and more detailed explanations were given in [14]. Additionally, the variables are listed and a mathematical mixed-integer linear programming (MILP) model is proposed for each of the components. The model is used to optimize system operation by implementing energy-flexibility measures corresponding to the values defined in the EFDM. As a proof of concept, this paper aims to show that the EFDM approach can generally be applied to production systems. To simplify the optimization, this exemplary model does not consider all of the possible variables provided in the EFDM framework. The following assumptions are made:

- Each component can only assume one of the different power states: P^i with $i \in \{\text{upper}, \text{lower}, \text{reference}, \text{working}\}$
- The reference power state $P^{\text{reference}}$ is not considered in the optimization model and is merely used to evaluate energy-flexibility measures in Section 6 of this paper.
- Regeneration duration t_R is not modelled.
- The power gradients ∇P_{Act}, ∇P_{Mod}, and ∇P_{Dea} are not modelled.
- Target energy contents for flexible storages E_{Tar} are not considered in the optimization model.
- Costs c_S associated with storage operation are not considered.
- Dependencies between multiple flexible loads are not modelled explicitely and only indirectly represented by flexible storages.

In addition to the existing variables, the following variables are introduced for keeping track of global figures:

- t: the number of current time steps;
- a: the width of a time step in seconds;
- T_{max}: the optimization horizon;
- c^{el}: the cost of electricity at time t.

In the following section, we introduce all of the components of the EFDM and the respective equations describing their behavior.

*A **Flexible Load** models a technical system or the interaction of different technical systems that have the potential to produce a change in performance [14].*

The key figures for describing a flexible load are shown in Table 1.

Table 1. Description of the key figures in the energy flexibility data model (EFDM) of flexible loads, following [6].

Key Figure	Description
$\mathbb{L}$	Set of all flexible loads *id*
id	Flexible load ID
t_{D}	Reaction duration
T_{V}	Validity
$\mathbf{P}_{id}$	Power states
t_{H}	Holding duration
N_{A}	Usage number
N_{Mod}	Modulation number
∇P_{Act}	Activation gradient
∇P_{Mod}	Modulation gradient
∇P_{Dea}	Deactivation gradient
t_{R}	Regeneration duration
c_L	Cost for operation of flexible load

The set of all flexible loads is defined as $\mathbb{L}$. The momentary power consumption P of a flexible load is described by

$$P_{id,t} = b_{id,t} \cdot \left(P_{id}^{\mathrm{upper}} - P_{id}^{\mathrm{lower}} \right) + P_{id}^{\mathrm{lower}} \quad \forall t, \forall id \in \mathbb{L} \tag{1}$$

and with

$$\left.\begin{aligned} b_{id,t}^{\mathrm{start}} &\geq b_{id,t} - b_{id,t-1} \\ b_{id,t}^{\mathrm{end}} &\geq b_{id,t-1} - b_{id,t} \end{aligned}\right\} \quad \forall t, \forall id \in \mathbb{L} \tag{2}$$

the binary parameters b^{start} and b^{end} can be equate to 1 if the load is switched on or off, respectively.

Once the flexible load reaches the upper power state, it must remain at that state for the duration t_H^{upper}, as constrained by

$$b_{id,t}^{\mathrm{end}} \cdot \left(t_H^{\mathrm{upper}} - \sum_{T=t}^{t-t_H^{\mathrm{upper}}} b_{id,T} \right) \leq 0 \quad \forall t, \forall id \in \mathbb{L} \tag{3}$$

The same applies for the lower power state, as constrained by

$$b_{id,t}^{\mathrm{start}} \cdot \left(t_H^{\mathrm{lower}} - \sum_{T=t}^{t-t_H^{\mathrm{lower}}} b_{id,T} \right) \leq 0 \quad \forall t, \forall id \in \mathbb{L} \tag{4}$$

where the flexible load must remain for t_H^{lower} seconds. Equation (5) ensures that the maximum number of usages allowed by the EFDM of the component is not exceeded.

$$\sum_{t=0}^{T_{\max}} b_{id,t}^{\mathrm{start}} \leq N_A \quad \forall t, \forall id \in \mathbb{L} \tag{5}$$

Finally, the total operating cost of a flexible load over the optimization horizon is determined by

$$c_{L,id} = \sum_{t=0}^{T_{\max}} \left(a \cdot P_{id,t} \cdot c_t^{\mathrm{el}} \right) \quad \forall id \in \mathbb{L}. \tag{6}$$

Flexible loads could interact with one or more storages, as we describe in the following.

*An **Energy-Storage** system is a technical system or the interaction of different technical systems that have the potential to store energy. In general, in addition to direct energy storage*

systems, such as heat storage or battery storage, inherent storage such as product storage is also possible. Energy storage cannot be used for energy flexibility without flexible loads since no power change is possible without a flexible load [14].

The energy storage is described by the key figures given in Table 2.

Table 2. Description of the key figures in the EFDM of storages, following [6].

Key Figure	Description
$\mathbb{S}$	Set of all energy storages *id*
id	Storage ID
C_S	Usable capacity
E_{t0}	Initial energy content incl. time stamp
E_{Tar}	Target energy content incl. time stamp
E_{Loss}	Energy loss
S_S	Suppliers
E_S	Drain
c_S	Cost for operation of flexible storage

The set of all available energy storages is defined as $\mathbb{S}$. The current energy content E of an energy storage is defined by

$$E_{id,t} = E_{id,t_0} + \sum_{t=0}^{t} a \cdot \left(S_{S,id,t} - E_{S,id,t} - E_{Loss,id}\right) \quad \forall t, \forall id \in \mathbb{S} \tag{7}$$

A storage's energy content cannot exceed its capacity C_S or fall below its minimum energy content C_S^{min}, so

$$C_{S,id}^{min} \leq E_{id,t} \leq C_{S,id} \quad \forall t, \forall id \in \mathbb{S} \tag{8}$$

it is given as constraint. Lastly, dependencies describe the relations between multiple flexible loads. Dependencies can be used if switching one flexible load also requires changes from another flexible load.

The class ***Dependencies*** *can be used to model constraints and dependencies for the interaction of multiple flexible loads. For example, the use of one flexible load can imply or exclude the use of another flexible load.*

The key figures to describe those dependencies between flexible loads does not occur in our use case, so we refer to [6].

In addition to the three classes mentioned above for describing the Flexibility Space, a flexible load measure (FLM) describes a concrete performance change of the system within its flexibility space [6,15].

A ***Flexible Load Measure*** *describes a deliberate action taken to implement a defined change of state in a production system and encompasses the change in state of a production station and the interactions in the production system which this change entails. This is accompanied by a concrete change in performance within the flexibility space, no longer has any degrees of freedom itself, and is time-terminated.*

The key figures to define a FLM are given in Table 3, and an exemplary representation is shown in Figure 2.

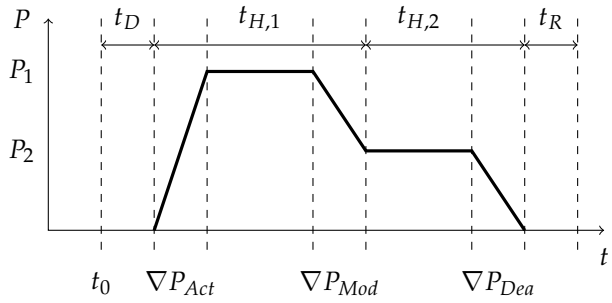

Figure 2. Simplified representation of an FLM.The figure shows the meaning of the key figures, which are given in Table 3.

Table 3. Description of the key figures in the EFDM of flexible load measure, following [6].

Key Figure	Description
id	Flexible load measure ID
t_{D}	Reaction duration
t_0	Starting time
$\mathbf{P}_{id}$	Power states
t_{H}	Holding duration
N_{A}	Usage number
$\nabla\mathbf{P}$	Vector of gradients
c_M	Cost for flexible load measure

2.2. Production Scheduling

Since this paper considers demand-response measures for technical supply systems in connection to production equipment, it is necessary to take production scheduling into account. In our study, grinding machines are modeled in the EFDM context, so there are some specific properties that must be incorporated.

We assume that the grinding machine is part of a flow production line that is configured so that production flows consistently. Therefore, takt time t_{takt} is the quotient of available working time divided by customer demand [16]. In our case, demand is defined by an overall production capacity utilization of approximately 70%, meaning the production line is not utilized for 30% of the available time.

One machine in the production line is considered for the demand-response optimization. This leads to the machine becoming a potential bottleneck in the production line. Therefore, the scheduling problem can be considered to be a single machine scheduling problem, which is solved offline [17]. Possible changes, for example, resulting from equipment breakdowns, are not accounted for.

Given these simplifications, we apply the above-mentioned models to the grinding machine with the exception that workpieces are discrete units. Therefore, Equation (7) must be mapped to discrete steps so that

$$E_{id,t} = E_{id,0} + \left\lfloor \sum_{t=0}^{t} S_{S,id,t} - E_{S,id,t} - E_{Loss,id} \right\rfloor \quad \forall t, \forall id \in \mathbb{S} \tag{9}$$

follows.

2.3. Virtual Sensors and Pump Theory

In order to quantify the interaction between the grinding machine and the cooling-supply system in form of the EFDM of the cold storage, the cooling demand of the grinding machine is required. Apart from installing a physical metering device to directly measure the volume flow of the cooling medium, a virtual sensor can be introduced to calculate the volume flow from other measured signals. This approach is especially advantageous if

purchasing, implementing, and maintaining a physical sensor is expensive [18]. As physical volume flow sensors are usually either invasive, requiring one to open the system for installation (e.g., paddle wheel volumetric flow meters [19]), or expensive (e.g., ultrasonic volumetric flow meters [20]), a virtual sensor is developed to acquire the cooling medium volume flow.

According to [21], there is currently no uniform definition of virtual sensors. In [22], virtual energy metering points are subdivided into

- Aggregation and disaggregation approaches,
- Hybrid modeling approaches,
- Approaches based on physical modeling.

Hybrid virtual energy consumption models are characterized as empirical models based on conditional or process data [22]. In the presented case, we use such a hybrid approach to develop the virtual energy metering point. In the ETA Research Factory [23], intelligent pumps (Grundfos Magna3 [24]) containing internal metering points for electric load and rotational speed are installed. These signals are used as inputs for a data-based model to predict the pump volume flow. In order to develop the model, the volume flow is temporarily measured using a physical ultrasonic sensor (Flexim F601 [25]). This temporary measurement is then used as target value for data-based modeling.

The relation between the predicted volume flow and the cooling demand needed for the EFDM is derived from the first law of thermodynamics so

$$\begin{aligned} \dot{Q} &= \dot{m} \cdot c_p \cdot \Delta T \\ &= \dot{V} \cdot \rho \cdot c_p \cdot (T_{\text{outlet}} - T_{\text{inlet}}) \end{aligned} \tag{10}$$

following [26] for the heat flux, which is equivalent to the cooling demand over time $\dot{Q}$.

With the density ρ and specific heat capacity c_p assumed as constant material properties of the flow medium, the heat flux depends solely on the volume flow $\dot{V}$ and the temperature difference between the inlet and outlet temperature $\Delta T = T_{\text{outlet}} - T_{\text{inlet}}$. Since the temperature difference can be measured directly with little effort, the volume flow is the only missing property to obtain the heat flux describing the cooling demand of the grinding machine.

Following the similarity laws of pumps given in [27], the volume flow of centrifugal pumps is dependent on the rotational speed, the pressure difference, and the electrical load. While all of these parameters are dependent on each other, it is usually sufficient to know two of them to fully describe a pump state [27]. However, since all three of the parameters are provided by the intelligent pump utilized in this work, all three are used as input parameters to model the volume flow.

Without knowledge of the pump efficiency in each pump state, the dependency between the mentioned parameters cannot be explained with physical equations [27]. Therefore, a data-based model is needed. The development of this model is described in Section 4, and it is subsequently used in Section 6 to obtain the heat flux between the systems.

3. Experimental Setup

The fundamentals covered in Section 2 lay the foundation for implementing an EFDM in [6] to a physical industrial setting for evaluating its practicality. The equipment used is located in the ETA Research Factory (Technical University of Darmstadt) [23], which is a research facility focused on energy efficiency and flexibility in industrial applications.

In the following section, the use case and utilized equipment are presented. The setting revolves around a vertical CNC grinding machine for the precision machining of pump-control disks as part of the ETA Research Factory process chain. After turning, cleaning, drying, and heat treatment, the parts arrive at the grinding machine as the last machining process before final cleaning.

3.1. Grinding Machine

The examined grinding machine is a highly automated vertical CNC grinding machine for high-volume production including an integrated pick-up automation system [28] as shown in Figure 3. It is part of a level flow production line as described in Section 2.2.

Figure 3. Picture of the CNC grinding machine of the use case for the energy-flexible operation.

In addition to the grinding machine, the experimentation scope also includes the grinding machine's cooling supply and workpiece storage. The grinding machine contains several components requiring cooling in order to maintain process quality and component durability and performance. These components include the turning spindle, the two grinding spindles, and the cooling lubricant supply. In addition, the control cabinet needs to be cooled during operation. Cooling is circulated within the machine via a temperature controlled internal cooling circuit. Cooling energy is externally supplied by the central cooling system through a heat exchanger.

3.2. Cooling System

The cooling-supply system consists of a cooling circuit and an air-chiller unit [29] providing it with cooling energy. The circuit includes a thermal buffer storage [30], which adds thermal inertia to the system for added flexibility. Cooling energy is transported from the chiller to the cold storage and from the cold storage to the grinding machine by means of pumps and heat exchangers. Cold flux is calculated using a virtual volume-flow sensor, which is described in detail in Section 4. Since the cooling lubricant supply is separated from the grinding machine, it has its own internal cooling system, which is also supplied by the central cooling circuit. The average cooling demand during production is approximately 477 W at a cooling temperature of 20 °C. Cooling energy is transported from the cooling circuit to cooling energy consumers by centrifugal pump 2 [24], as seen in Figure 4.

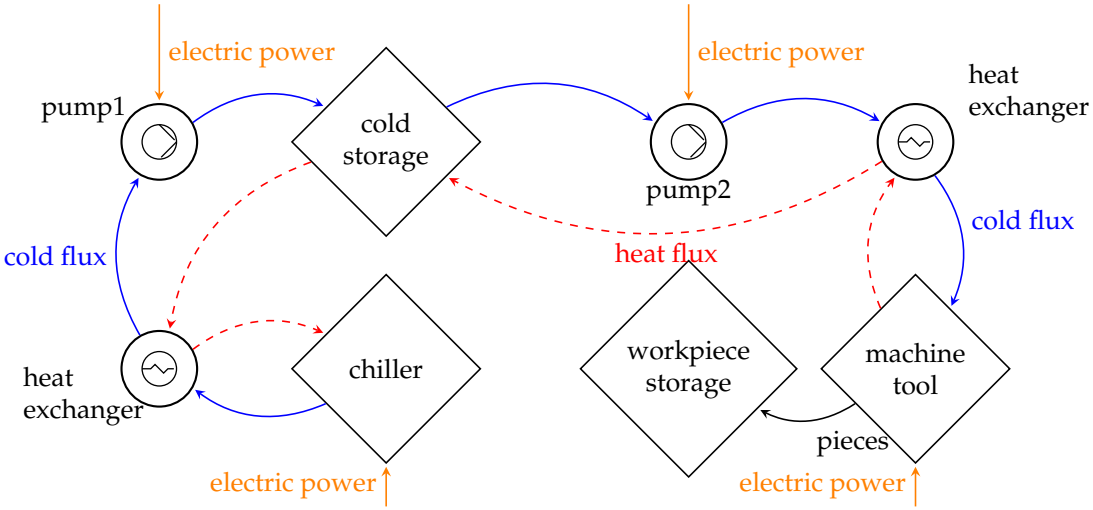

Figure 4. This schematic experimental setup shows the dependencies between the subsystems.

The network is cooled to a temperature range of 18–22 °C by means of the chiller. The internal cooling circuit of the chiller transfers cooling to the chilled water network through a heat exchanger and has a nominal cooling power of 6 kW (at $T_{supply} = 18$ °C and $T_{ambient} = 35$ °C). On the other side of the heat exchanger, centrifugal pump 1 [24] transports the chilled water throughout the network. The chiller is operated by being given a target temperature to reach via bang-bang control, while compensating thermal loads to maintain the target temperature. As a result, the chiller usually demonstrates variable electrical power consumption, depending on how far it is from the target temperature.

To increase the flexibility of the chilled water system, a thermal buffer storage is installed, which also acts as a hydraulic separator to decouple pumps installed in the network. The storage allows for charging at different heights in order to separate different temperature levels and reduce exergy losses. The storage is thermally insulated and allows temperatures as high as 90 °C and as low as freezing temperature with a volume of 950 L. However, only a temperature range of 10 °C to 30 °C is required for the following use-case. A schematic of the experimental setup is shown in Figure 4.

3.3. Production System

The production line considered in this paper consists of five workcenters. Production begins with milling and turning operations and continues with a cleaning step followed by heat treatment. After heat treatment, parts are ground in the grinding machine followed by a final cleaning process. This paper only considers the grinding machine, as it is the bottleneck of the production line as described in Section 2.2. The key parameters of the machine can be determined using the takt time t_{takt} of the production line, which is 101 s as defined in Section 2.2 in this case. For level production, three grinding machines are required in the production line. For the purpose of this paper, only one of these three machines is considered. This leads to a machine cycle time of 303 s.

The grinding machine has a workpiece storage for finished workpieces. This storage must never be completely empty to ensure continuous operation of the subsequent machines is not interrupted. This storage has a capacity of 20 parts and supplies the subsequent production processes, which require seven pieces every 2016 s from the considered grinding machine, as shown in more detail in Section 5.1.

3.4. Energy Flexibility Components

The aforementioned components represent the three subcategories of the energy-flexibility data model—flexible loads, storages and dependencies—as described in Section 2 to constitute a flexibility space [6]. In the use-case, both the grinding machine [28] and the

chiller [29] represent flexible loads, due to their consumption of electrical power. Linked to these flexible loads are corresponding storages. In the case of the chiller, the storage is represented by the thermal buffer storage [30] since it stores cooling energy. The workpiece storage, storing finished parts from the grinding machine, also acts as storage. Although parts are not directly comparable to thermal or electrical energy stored in a reservoir, they are considered in order to flexibilize not only the cooling supply but also the supply in the finished parts and this part of the process chain. Dependencies, which should exist between flexible loads, are not represented in the use-case since the only flexible loads within the presented experimental scope (grinding machine and chiller) are only indirectly connected through the chilled water network and the thermal buffer storage [6]. However, boundary conditions, which ensure realistic operation, are considered in Section 5.

4. Development and Modelling of a Virtual Volume-Flow Sensor

As described in Section 2, the volume flow of cooling medium and thereby heat flux is obtained using a virtual sensor in this work. The virtual sensor is developed for pump 1 (see Figure 4), which is speed-regulated and therefore has adaptive operating states. Pump 2, on the other hand, operates in a constant operational state, which is why its volume flow is assumed constant at 0.617 m^3/h. The virtual sensor of pump 1 essentially consists of a data-based model with the properties of rotational speed and electric load as inputs and the volume flow as output (see Figure 5).

Figure 5. Schematic of the virtual volume-flow sensor. The virtual sensor takes the electric load and rotational speed of the pump as inputs and computes the corresponding volume flow.

Three different methods to estimate the volume flow are developed and compared within this work:

1. A physical model based on the characteristic diagram provided by the pump supplier;
2. A statistical model using linear regression;
3. A machine learning model.

These three methods represent different modeling strategies typically used in energy modeling [31].

For the first method, the physical model and the characteristic diagrams are provided in the data sheet by the pump manufacturer [24]; they visualize whether the dependency between the volume flow, electric load, and rotational speed of the pump is read into a table format using an image-recognition algorithm. The pump state is then determined by linear interpolation between the known characteristic lines of the pump given in these diagrams. As input parameters, the electric load and the rotational speed, represented by the relative pump power in %, are used. This approach is based on the information provided by the pump manufacturer, which is an approximation of the real pump states. The advantage is that no temporary measurement is needed, but the results (Table 4) show that this approach is the least accurate of the three.

The second and third method are both data-based methods based on the temporary measurement of the volume flow with the ultrasonic metering device Flexim F601 [25]. To capture as many system states as possible within the training data set, the pump states are manually altered between measurements by setting the control signal to relative power states between 0 and 100%. The corresponding valve is kept completely open during the measurements since this is always the case during pump operation in the examined system. The training data set is displayed in Figure 6.

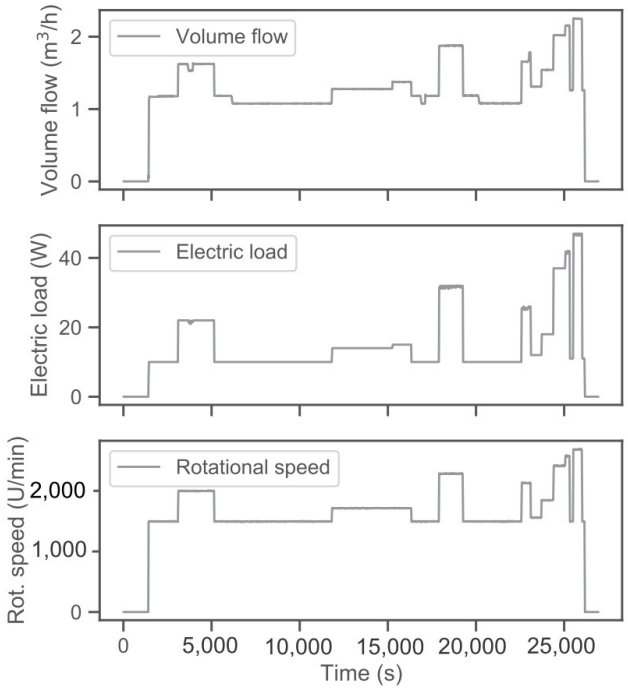

Figure 6. Training data for modeling the virtual sensor with the data-based approaches. The different graphs show the input and output signals introduced in Figure 5. (**Top**): volume flow (output), (**center**): electric load (input 1), and (**bottom**): rotational speed (input 2).

The data set is prepared before training by removing missing values and outliers. For outlier detection, a method based on the median absolute deviation from the median within a rolling window of seven values is used [32].

The linear regression model represents a simple but robust and transparent method to predict the volume flow. This involves a linear equation with unknown coefficients r_0, r_1, and r_2, which is set up to compute the volume flow

$$\dot{V} = r_0 + r_1 \cdot P_{\mathrm{el}} + r_2 \cdot \mathrm{n} \tag{11}$$

from electric load P_{el} and the rotational speed n. The coefficients r are determined by minimizing the cost function (sum of squared errors)

$$cost = \frac{1}{2k} \sum_{i=1}^{k} (y^{(i)} - \hat{y}^{(i)})^2 \tag{12}$$

with $y^{(i)}$ observations, $\hat{y}^{(i)}$ predictions, and k samples. The values of the coefficients allow for posterior analyses of the influencing factors of the volume flow to be carried out, and therefore for some insight into the model to be gained. Due to the linear characteristic, the model is unlikely to overfit the data, so this makes it robust [33]. The results in Table 4 show that this approach provides an accurate prediction and generalizes well to unseen data.

As a third method, a more sophisticated machine learning technique is used. Utilizing a probability-based hyperparameter optimization with the Python library *hyperopt* [34], a feedforward neural network and a gradient boosting regression tree (GBRT) algorithm are tested and evaluated. The GBRT is an ensemble of decision trees [35]. The hyperparameter search grid includes a variety of hyperparameters, including the network depth and the dropout rate for the neural network, as well as the number of estimators for the GBRT from the Python library *scikit-learn* [36]. As a result of the hyperparameter optimization, the GBRT algorithm is selected due to its superior performance on unseen data. It performs very well on the training data set but compared to the linear regression model is less

transparent and generalizes slightly worse to unseen data, as can be seen at its lower test score in Table 4.

The results of all of the models on unseen data are compared in Table 4. As a result, the linear model is selected as a virtual sensor for the volume flow of pump 1 since it performs well on the test data and is transparent. The predictions of the linear regression model on the test data are shown in Figure 7.

Table 4. Results of the volume flow modeling: comparison between the three approaches. Metrics: mean absolute error (MAE), root mean squared error (RMSE), and coefficient of determination (R^2-score).

Modeling Approach	MAE (m^3/h)	RMSE (m^3/h)	R^2-Score (-)
Interpolation model	0.159	0.306	0.876
Linear regression	0.108	0.206	0.943
GBRT	0.099	0.211	0.941

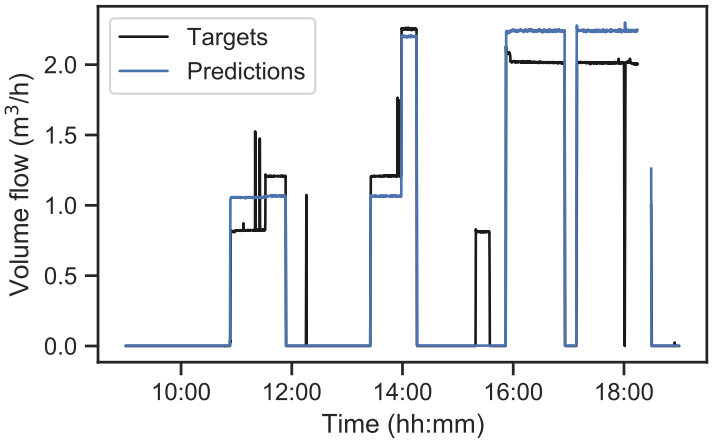

Figure 7. Predictions of the virtual sensor with the linear regression approach on unseen data.

5. Energy-Flexibility Data Model of the System

As mentioned in Section 3, applying the energy-flexibility data model to the use-case results in representations of two flexible loads (grinding machine and chiller) and two storages (thermal buffer storage and parts warehouse). As a first step, the data representation of each component is defined by determining key figures specified by [6].

5.1. Grinding Machine

To obtain the key figures of the grinding machine data model (see Table 5), test runs are conducted including transitions between the dominant machine states *working*, *reference*, and standby. The main data points observed are the active power intake of the grinding machine and the machine state. The second important data source is the production plan that determines how many parts are produced during the validity period. The following assumptions are made before determining the key figures:

1. The dominant machine states are *working* corresponding to P^{upper}, in which parts are produced, and *standby* corresponding to P^{lower}, in which the machine stands still and unnecessary auxiliary units are switched off. Between these two states, the state *reference* is defined in which parts are produced in the takt-time t_{takt} defined by production planning (without any flexibilitzation). The machine state *operational* (between *standby* and *working*) is regarded as purely transitional and is represented in the activation and deactivation gradients. The machine states *disabled* and *off* are not regarded in this study.
2. The mean power intake is assumed to be constant during the machine states.

3. Production can be halted after each finished part as long as the workpiece storage's limits are not breached.
4. To facilitate calculations and optimization, the machine is assumed to be in mode *standby* at the start of the shift and ready to produce.

The most important key figures are explained below:

The reaction duration t_D depends on the current power state. A signal latency of 0.5 s is defined as the minimal reaction duration. When transitioning from power states *working* or *reference* to *standby*, the reaction duration can assume values between 0.5 s and the cycle time of the workpiece in production (159 s) since production must be finished before being able to transition into another power state:

$$t_\mathrm{D} = \begin{cases} 0.5\,\mathrm{s}, \text{if } P^{\text{standby}} \rightarrow P^i \\ [0.5\,\mathrm{s}, 159\,\mathrm{s}], \text{if } P^{\text{reference}} \rightarrow P^i \\ [0.5\,\mathrm{s}, 159\,\mathrm{s}], \text{if } P^{\text{working}} \rightarrow P^i \end{cases} \tag{13}$$

The validity T_V is determined by the production shift:

$$T_\mathrm{V} = \begin{array}{l}[[16.04.2020\ 06{:}00{:}00,\ 16.04.2020\ 11{:}00{:}00],\\ [16.04.2020\ 12{:}00{:}00,\ 16.04.2020\ 14{:}00{:}00]]\end{array} \tag{14}$$

The power state vector $\mathbf{P}_{id}$ is generally defined as

$$\mathbf{P}_{id} = \begin{pmatrix} P^1 \\ P^2 \\ \vdots \\ P^i \end{pmatrix} \tag{15}$$

so in our case for each mean power intake in each dominant state

$$\mathbf{P}_{id} = \begin{pmatrix} P^{\text{standby}} \\ P^{\text{reference}} \\ P^{\text{working}} \end{pmatrix} = \begin{pmatrix} 1.592\,\mathrm{kW} \\ 3.889\,\mathrm{kW} \\ 5.186\,\mathrm{kW} \end{pmatrix} \tag{16}$$

results.

Possible holding durations t_H are defined by the system characteristics and responsible persons and depend on the assumed power state. A minimum of 30 s holding duration is defined to prevent high-frequency state changes. In *working* and *reference*, the holding durations are discrete and consist of multiples of the respective takt or process time. Maximum holding duration is the product of takt or process time and planned product in validity time. In *standby*, any holding durations above the minimum can be assumed.

$$t_\mathrm{H} = \begin{cases} P^{\text{standby}} : [30\,\mathrm{s}, \mathrm{inf}) \\ P^{\text{reference}} : \{1 \cdot 302\,\mathrm{s}, 2 \cdot 302\,\mathrm{s}, \ldots, 123 \cdot 302\,\mathrm{s}\} \\ P^{\text{working}} : \{1 \cdot 159\,\mathrm{s}, 2 \cdot 159\,\mathrm{s}, \ldots, 123 \cdot 159\,\mathrm{s}\} \end{cases} \tag{17}$$

The usage number, the number of uses of the flexible load in the planning horizon,

$$N_\mathrm{A} = 123 \tag{18}$$

is determined by the production plan. The power states can be changed at most as many times as parts are planned for the shift.

Since each change (activation and deactivation) is regarded as one usage, no modulations of the power state can be achieved during the usage. Therefore,

$$N_{\mathrm{Mod}} = 0 \tag{19}$$

is defined.

The activation gradient denotes the power gradient of the transition from the *reference* load profile to another state, i.e., activating a certain flexibility measure. The transition times between states are determined experimentally. Between *reference* and *working*, the transition time is 0.0 s. From *reference* to *standby*, transition time is 376.0 s. The gradient can thus be calculated by dividing the difference between the power states by the transition time, resulting in

$$\nabla P_{\mathrm{Act}} = \begin{pmatrix} P_{act}^{\mathrm{working}} \\ P_{act}^{\mathrm{standby}} \end{pmatrix} = \begin{pmatrix} \inf \\ -6.1\,\mathrm{W\,s^{-1}} \end{pmatrix}. \tag{20}$$

Similarly, the deactivation gradient from *working* or *standby* back to *reference* is determined. The transition time from *working* to *reference* is 0.0 s, while it is 46.0 s from *standby* to *reference*. This results in the

$$\nabla P_{\mathrm{Dea}} = \begin{pmatrix} P_{dea}^{\mathrm{working}} \\ P_{dea}^{\mathrm{standby}} \end{pmatrix} = \begin{pmatrix} -\inf \\ 50.0\,\mathrm{W\,s^{-1}} \end{pmatrix}. \tag{21}$$

Concerning the modulation gradients, it applies that for

$$N_{\mathrm{Mod}} = 0 \Rightarrow \nabla P_{\mathrm{Mod}} = \{\}.$$

The regeneration duration t_{R} denotes the time until the FLM can be activated again after deactivation. In the case of the grinding machine, this waiting period is set to zero since all relevant constraints (the remaining production time and latency in the reaction duration; the gradients and workpiece storage capacity; and the production plan) are already covered in other key figures of the grinding machine or workpiece storage data model.

The costs are an important factor in evaluating whether or not to activate a proposed FLM. They denote the additional costs that result from activating the measure. In the case of the grinding machine, the following costs should be taken into account:

- Additional wear and tear due to additional start-up and powering-down;
- Possible workpiece quality reduction due to additional start-up phases and required rework or additional production rejects;
- Costs that result from a possibly higher risk of production downtime due to the operation of the system energy flexibly.

The wear and tear costs, the quality-related costs, and the risk costs are not easy to determine. Further studies in this field are required to provide reliable values. Therefore, the costs are assumed to be zero in the presented study since it focuses on the technical aspects of flexibility modeling with reduced complexity.

Table 5. Specified EFDM of the grinding machine.

Key Figure	Calculation Rule	Grinding Machine	Units
id	Assigned by central system	Emag_gt	-
t_{D}	Defined by system characteristics	0.5 s, if $P^{\mathrm{standby}} \rightarrow P^{i}$ [0.5 s, 159 s], if $P^{\mathrm{preference}} \rightarrow P^{i}$ [0.5 s, 159 s], if $P^{\mathrm{working}} \rightarrow P^{i}$	s
T_{V}	Assigned by system responsible person	[[16.04.2020 06:00:00, 16.04.2020 11:00:00], [16.04.2020 12:00:00, 16.04.2020 14:00:00]]	s
$\mathbf{P}_{id}$	$P_i = \mathrm{mean}_t(P_i(t))$	$P^{\mathrm{standby}} = 1.5921$ $P^{\mathrm{preference}} = 3.8895$ $P^{\mathrm{working}} = 5.1864$	kW
t_{H}	Defined by system characteristics	$P^{\mathrm{standby}} : [30\ \mathrm{s}, \mathrm{inf})$ $P^{\mathrm{preference}} : \{1 \cdot 302\ \mathrm{s}, 2 \cdot 302\ \mathrm{s}, \ldots, 123 \cdot 302\ \mathrm{s}\}$ $P^{\mathrm{working}} : \{1 \cdot 159\ \mathrm{s}, 2 \cdot 159\ \mathrm{s}, \ldots, 123 \cdot 159\ \mathrm{s}\}$	s
N_{A}	Defined by system characteristics	123	-
N_{Mod}	Defined by system characteristics	0	-
∇P_{Act}	$P^{i}_{act} = \frac{P^{i} - P^{\mathrm{initial}}}{t_{\mathrm{transition}}}$	$P^{\mathrm{working}}_{act} = \mathrm{inf}$ $P^{\mathrm{standby}}_{act} = -0.0061$	$\mathrm{kW\,s^{-1}}$
∇P_{Mod}	$P^{(i->j)}_{mod} = \frac{P^{j} - P^{i}}{t_{\mathrm{transition}}}$	-	$\mathrm{kW\,s^{-1}}$
∇P_{Dea}	$P^{i}_{dea} = \frac{P^{\mathrm{initial}} - P^{i}}{t_{\mathrm{transition}}}$	$P^{\mathrm{working}}_{dea} = -\mathrm{inf}$ $P^{\mathrm{standby}}_{dea} = 0.05$	$\mathrm{kW\,s^{-1}}$
t_{R}	Defined by system characteristics	0	s
c_L	Amount of start-ups cost per start-up	0	€

5.2. Chiller

Key figures for the chiller data model are derived through the observation of operation data, including cooling capacity, electrical energy consumption, the energy efficiency ratio (EER), and the actual and target temperatures—all of which are constantly monitored and recorded and represented, respectively, in Figure 8b. Therefore, the EER is calculated by following [37].

$$EER = \frac{\text{Cooling power}}{\text{Electrical power consumption}}. \tag{22}$$

Key figures, mentioned in Table 6, such as *power states* are limited by data from the technical specifications of the chiller. The key figures *reaction duration*, *modulation gradients*, and *activation gradient* are deducted from data generated in experimental operation of the chiller. Due to the nature of the cooling unit, deriving values for power gradients is not only dependent on target values but also depends on actual values in addition to demonstrating a typical hysteresis curve. The operation of the chiller is controlled by setting a target temperature, which in the use-case is 20 °C, as required by the grinding machine.

Based on the mentioned experimental operation and under the consideration of the associated valves, $t_{\mathrm{D}} = 60\,\mathrm{s}$ is defined. According to the EFDM of the grinding machine, the validities should be equal. The possibility of the continuous setpoint setting of the chiller affects the power states in that they can be variable in the interval $\mathbf{P}_{id} \in [0.8, 6]$ kW. This property—specifically, the bang-bang-control—also infects the holding duration of the chiller, which is why the value is defined as $t_{\mathrm{H}} = inf$. The same applies to the key figures N_{A} and N_{Mod}. The determination of the gradients is based on the measurements of the experimental operation (cf. Figure 8b) and is correspondingly

$$\nabla P_{\mathrm{Act}} = \frac{P_i - P_{\mathrm{initial}}}{t_{\mathrm{transition}}} = \frac{1815.99\,\mathrm{W}}{1560\,\mathrm{s}} = 1.164\,\mathrm{kW\,s^{-1}} \tag{23}$$

$$\nabla P_{\text{Mod}} = \frac{P_j - P_i}{t_{\text{transition}}} = \frac{180.27\,\text{W}}{830\,\text{s}} = 0.217\,\text{kW}\,\text{s}^{-1} \tag{24}$$

$$\nabla P_{\text{Dea}} = \frac{P_{\text{initial}} - P_i}{t_{\text{transition}}} \tag{25}$$

to be calculated. In this case, for $\nabla P_{\text{Dea}} = inf$, $t_{\text{R}} = 0\,\text{s}$ is chosen because of the immediate switch-off behavior of the chiller.

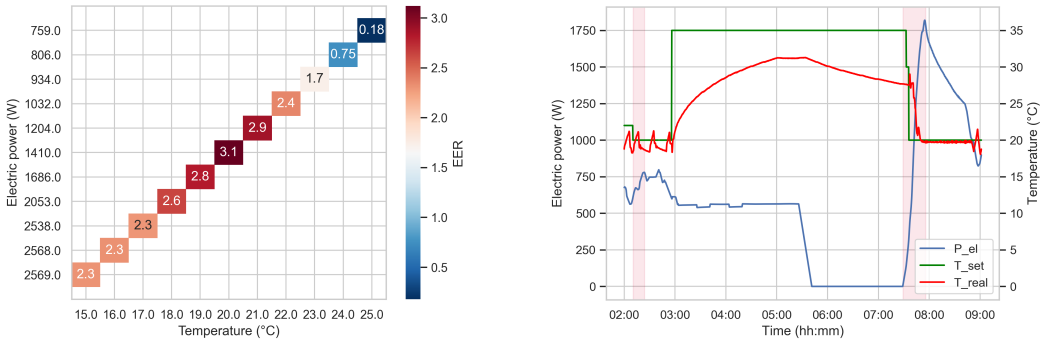

(**a**) (**b**)

Figure 8. Here, (**a**) shows a heatmap that represents the correlation of the EER of the chiller on the set temperature T_{set} and the electrical power used. (**b**) shows the electrical power time series of the chiller, while in the marked areas the gradients of the EFDM are calculated. Over the first marked time period, ∇P_{Mod} is calculated, and over the second time period ∇P_{Act} is calculated.

Table 6. Specified EFDM of the chiller.

Key Figure	Calculation Rule	Chiller	Units
id	Assigned by central system	Chiller	-
t_{D}	Defined by system characteristics	60	s
T_{V}	Assigned by system responsible person	[[16.04.2020 06:00:00, 16.04.2020 11:00:00], [16.04.2020 12:00:00, 16.04.2020 14:00:00]]	s
$\mathbf{P}_{id}$	$P_i = \text{mean}_t(P_i(t))$	[0.8, 6]	kW
t_{H}	Defined by system characteristics	inf	s
N_{A}	Defined by system characteristics	inf	-
N_{Mod}	Defined by system characteristics	inf	-
∇P_{Act}	$\nabla P_{\text{Act}i} = \frac{P_i - P_{\text{initial}}}{t_{\text{transition}}}$	0.0024	$\text{kW}\,\text{s}^{-1}$
∇P_{Mod}	$\nabla P_{\text{Mod}\,(i->j)} = \frac{P_j - P_i}{t_{\text{transition}}}$	0.0016	$\text{kW}\,\text{s}^{-1}$
∇P_{Dea}	$\nabla P_{\text{Dea}i} = \frac{P_{\text{initial}} - P_i}{t_{\text{transition}}}$	inf	$\text{kW}\,\text{s}^{-1}$
t_{R}	Defined by system characteristics	0	s
c_L	Number of startups cost per startup	0	€

5.3. Cold Storage

The key figures of the cold storage, mentioned in Table 7, need to be defined, so we can create the full EFDM of the experimental setup. The calculation rules for each key figure are defined in Table 8, and some more detailed information is given in the following. At first, we define the *id* for the storage as "cold storage". The different temperature values of the storage are used are T^v_{stor} with $v \in \mathbb{V}$, whereby

$$\mathbb{V} = \{\text{cmax}, \text{cmin}, \text{start}, \text{tar}, \text{max}, \text{min}\}$$

applies, whereby:

cmax ≡	The critical maximum temperature;
cmin ≡	The critical minimal temperature;
start ≡	The start temperature;
tar ≡	The target temperature;
max ≡	The maximum temperature of flexible operation;
min ≡	The minimum temperature of flexible operation .

The capacity of the used storage is calculated by

$$C_{\mathrm{S}} = m_{\mathrm{stor}} \cdot c_p \cdot \frac{T_{stor}^{cmax} - T_{stor}^{cmin}}{r_{\mathrm{u}}} \tag{26}$$

with the mass of the storage medium $m_{\mathrm{stor}} = 1000\,\mathrm{kg}$. As mentioned the storage medium is water, so $c_p = 4.184\,\mathrm{kJ\,kg^{-1}\,K^{-1}}$ is used [38]. Furthermore, the temperature range is so selected that its is permissible for the production process and thus follows $T_{stor}^{cmax} = 18\,^{\circ}\mathrm{C}$ and $T_{stor}^{cmin} = 22\,^{\circ}\mathrm{C}$. To obtain the storage capacity in the EFDM defined form, we need $r_u = \frac{1}{3600}$ for the conversion between J and W h so that from Equation (26) the capacity range

$$C_{\mathrm{S}} = [0, 4.648]\mathrm{kWh} \tag{27}$$

follows. To calculate the initial energy content of the used storage, we take into account the actual storage temperature $T_{stor}^{start} = 20\,^{\circ}\mathrm{C}$, and we define $T_{stor}^{min} = 20\,^{\circ}\mathrm{C}$ as our lower desired temperature in the experimental setup. Based on this

$$E_{\mathrm{t0}} = m_{\mathrm{stor}} \cdot c_p \cdot \frac{T_{stor}^{start} - T_{stor}^{min}}{r_u} = 2.034\,\mathrm{kWh} \tag{28}$$

is the result for this key figure. In a similar way, the calculation

$$E_{\mathrm{Tar}} = m_{\mathrm{stor}} \cdot c_p \cdot \frac{T_{stor}^{tar} - T_{stor}^{min}}{r_u} = 0\,\mathrm{kWh} \tag{29}$$

with the defined value $T_{stor}^{tar} = 18\,^{\circ}\mathrm{C}$. To take unavoidable energy losses E_{Loss} into account, the manufacturer-specific heat losses of the storage $q_{\mathrm{BS}} = 1.37\,\mathrm{kWh/24\,h}$ is given [39]. In addition to the total volume $V = 1000\,\mathrm{L}$ and

$$\Delta T = T_{stor}^{cmax} - T_{stor}^{cmin} \tag{30}$$

the energy loss of

$$E_{\mathrm{Loss}} = \frac{q_{\mathrm{BS}}}{V \cdot c_p \cdot \rho \cdot \Delta T} = 1.228\,\%/\mathrm{h} \tag{31}$$

follows. For the determination of the efficiency indicator of the supply system of the cold storage—the chiller—the heatmap of Figure 8 is used to set $EER = 2.6$ for $T_{stor}^{tar} = 18\,^{\circ}\mathrm{C}$. Furthermore, the heat work required by the chiller by the grinding machine is assumed to be about 30% of the electric work given in Equation (16) and mentioned in Section 2.2, so that for one time step t

$$E_{\mathrm{S}} = 0.3 \cdot P_{\mathrm{GT},t} \tag{32}$$

follows.

Table 7. Specified EFDM of the workpiece storage.

Key Figure	Calculation Rule	Workpiece Storage	Units
id	Assigned by central system	Workpiece storage	-
C_S	Defined by system characteristics	20	pcs
E_{t0}	Defined by system state	10	pcs
E_{Tar}	Defined by system responsible person	7	pcs
E_{Loss}	Defined by system characteristics	0	$\% \, s^{-1}$
S_S	Supplier ID	Emag_gt	-
E_S	see Equation (33)	0.0035	pcs/s

Table 8. Specified EFDM of the cold storage.

Key Figure	Calculation Rule	Cold Storage	Units
id	Assigned by central system	Cold storage	-
C_S	$m_{stor} \cdot c_p \cdot \frac{T_{stor}^{cmax} - T_{stor}^{cmin}}{r_u}$	[0, 4.648]	kWh
E_{t0}	$m_{stor} \cdot c_p \cdot \frac{T_{stor}^{start} - T_{stor}^{min}}{r_u}$	(2.034, TS)	(kWh, s)
E_{Tar}	$m_{stor} \cdot c_p \cdot \frac{T_{stor}^{tar} - T_{stor}^{min}}{r_u}$	(0, TS)	(kWh, s)
E_{Loss}	$\frac{q_{BS}}{V \cdot c_p \cdot \rho \cdot \Delta T}$	$\frac{1.228}{3600}$	$\% \, s^{-1}$
S_S	(efficiency indicator, ID_Supplier)	(2.6, Chiller)	(-, -)
E_S	$(TS, 0.3 \cdot P_{GT,t})$	(16.04.2020 06:00:00, 0.477)	(s -> kW)
c_S	cost for operation of cold storage	0	€

5.4. Workpiece Storage

As described in Section 3.3, the workpiece storage has a capacity of

$$C_S = 20$$

workpieces. The initial content of the storage is determined by the current system state and is assumed to

$$E_{t0} = 10$$

pieces for the use case of this paper. Furthermore, the target energy content must be determined by a responsible person. In this case,

$$E_{Tar} = 7$$

is defined.

The supply S_S results directly from the produced workpieces of the grinding machine. Therefore, a coupling to this machine is required.

The drain from the requirements of the production line are described in Section 2.2. Specifically, the takt time t_{takt} and the number of machines are required to calculate the drain. The cleaning machines, which follow the grinding machine in the production process, require 20 pieces every 2016 s to keep the takt time of 101 s (see also Section 5.1). Since there are three grinding machines to fulfill this demand, each machine must supply 7 pieces every 2016 s.

$$E_S = \frac{7 \, \text{pcs}}{2016 \, \text{s}} = 0.0035 \, \text{pcs/s} \tag{33}$$

6. Application and Demonstration

Based on the optimization approach presented in Section 2 and the flexibility space created in Section 5, this chapter determines the energy cost-optimal flexible operation strategy and then implements it on the use case (e.g., Section 3). The results are then analyzed and discussed.

6.1. Energy Costs Optimal Flexible Operation

There are three steps to the application and demonstration. As a first step, the reference profile is measured. The result of this measurement is presented in Figure 9. Based on the measured reference load profile, the key figures for EFDM variables are determined, as shown in Section 5.

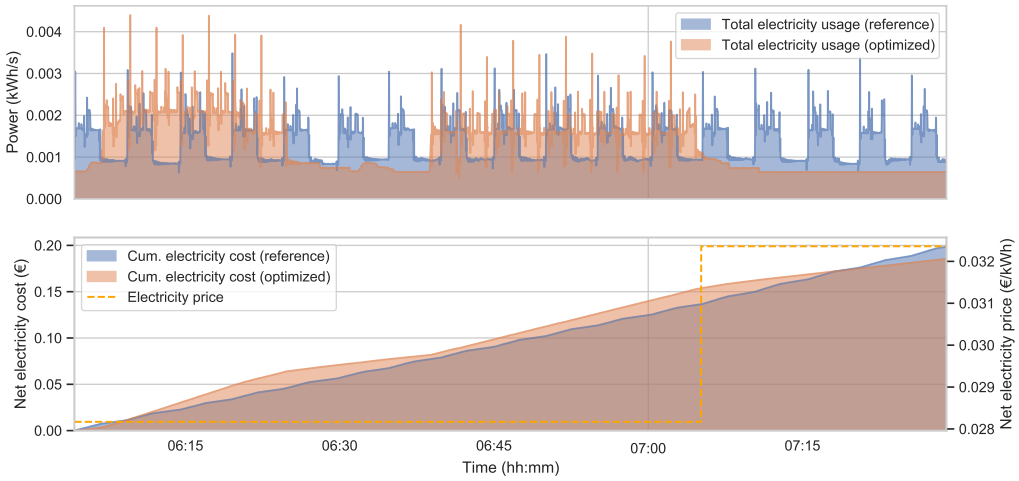

Figure 9. Comparison of the electricity cost of reference and optimized load profile. The upper graph shows the different operating modes and the load curve changed by the flexibilized and optimized operation. The resulting changes in electrical costs are shown in the lower graph. It can be seen that cost savings were achieved by making the production schedule more flexible.

With this reference profile, the optimization can be performed, which can in turn be utilized to perform a second experiment for the verification of the results. These are used in combination with the model proposed in Section 2 to determine when the grinding machine and the chiller should ideally operate.

Minimal electricity cost is used as an objective for the optimization. Day-ahead electricity prices in Germany from the 9 of January 2018 are used as a reference case for this. The electricity cost per machine is then calculated using

$$c_{L,id,t} = a \cdot P_{id,t} \cdot c_t^{\mathrm{el}} \tag{34}$$

which follows from Equation (6). Using Equation (34), the objective is to minimize the total electricity cost with

$$\min \sum_{id} \sum_{t}^{T_{\max}} c_{id,t} \quad . \tag{35}$$

Since the grinding machine and the chiller are connected by the cold storage, the cold storage fulfills a special role in this paper. The electric power consumption of the chiller and the grinding machine must be converted into heat power to enable the calculation of the energy content of the storage. The heat work performed by the chiller is equivalent to

the electric work $b_{ch,t} \cdot P_{ch,t} \cdot a$ times the EER. The heat work performed by the grinding machine is assumed to be about 30% of the electric work, so

$$\begin{aligned} E_{ch,t} = & E_{ch,t0} + \sum_{t=0}^{t} b_{ch} \cdot P_{ch,t} \cdot a \cdot EER_{ch} \\ & - E_{loss,ch} \cdot a \cdot t - 0.3 \sum_{t=0}^{t} \cdot P_{GT,t} \cdot a \end{aligned} \tag{36}$$

applies. Following the result of the optimization and the EFDM of the system, the FLM for the grinding machine is calculated. These calculations consist of an algorithmic solver. We use the industrial solver CPLEX by IBM [40] as the solver, which can solve MILP using different solving methods. The final result flexible load measure is described in Table 9 and exemplarily represented in Figure 10. For the implementation of the optimization results, the control signals were given manually to the machine tool and the chiller. In this way, the correct execution of the control signals could be guaranteed and errors in the data transmission could be excluded. The course of the implemented flexibility measure based on optimization can be seen in Figure 11. The results of the test to validate the optimization are considered below.

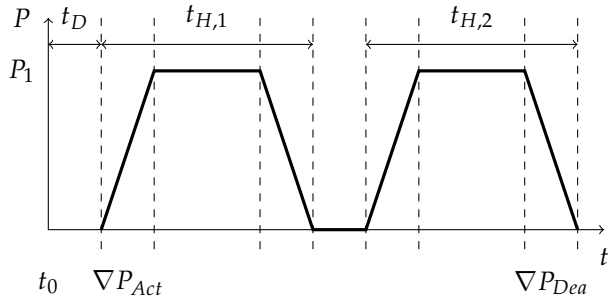

Figure 10. Simplified representation of the FLM for the grinding machine, which are given in Table 9.

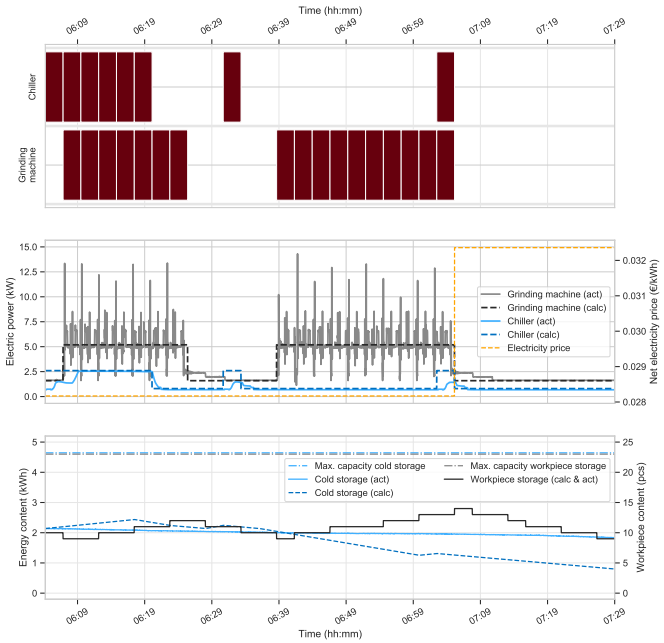

Figure 11. Results of the optimization. (**Top**): Control signal of the flexible loads chiller and grinding machine. (**Center**): Comparison of the electricity consumption of the flexible loads (calculated vs. actual) including the corresponding electricity prices. (**Bottom**): Comparison of the storage content of workpiece and cold storage (calculated vs. actual).

Table 9. Description of the key figures in the EFDM of flexible load measure, following [6].

Key Figure	Value	Units
id	Grinding Machine	-
t_D	159	s
t_0	[16.04.2020 06:00]	s
$\mathbf{P}_{id}$	[5.18]	kW
t_H	[4400]	s
N_A	2	-
$\nabla\mathbf{P}$	[inf, -, − inf]	kW s^{-1}
c_M	0.21	€

6.2. Discussion

The results of our model and the optimization are shown in Figure 11. The optimization horizon ranges from 6:00 am to 7:30 am, which includes one electricity price change from lower to higher prices at 7:00 am. The operating times of the grinding machine and the chiller are shown in the topmost graph of the figure. Due to the optimization, energy-consuming activities are mostly concentrated in the time range before this price change, when prices are lower. This is the expected result. While the number of produced workpieces in this time range is equal, the optimization reduced the energy cost by 6.6%. This is equivalent to a reduction in energy cost per piece by 1.9%. In addition to the energy costs saved, Biel and Glock [41] showed that the implementation costs of the approach demonstrated are low. Therefore, implementation according to the chosen approach is profitable due to the reduced energy costs.

The middle graph in Figure 11 shows that the energy consumption model of the grinding machine fits the actual data well. Small deviations result from disregarding gradients and load peaks. Such deviations are not relevant for the use case, if the total energy consumption is approximately correct.

The model of the chiller does not fit the actual data as well as the grinding machine model. For the chiller model, reaction times and gradients appear to have a larger influence. Therefore, future research should evaluate ways to model these factors. The capacity and energy loss of the cold storage have most likely been underestimated as well since the modeled energy content decreases faster than the measured values. This can be seen in the lower graph of Figure 11. These modeling errors do not invalidate the overall results, however, since improvements to the chiller and cold storage models would most likely lead to higher energy cost savings. These savings would result from shorter operating times of the chiller, resulting mostly from the higher cold storage capacity.

Figure 9 shows a comparison of the optimized energy consumption with the reference case. The energy consumption of the optimized case is aggregated into a shorter time frame, with longer pauses, while the reference case produces a very regular energy consumption pattern with shorter pauses. The upper graph in the figure also shows that additional effects resulting from longer pauses may contribute to the lower overall energy consumption. This may be due to machines changing into standby mode, thus reducing energy consumption.

The lower graph in Figure 9 shows cumulated energy consumption and the energy price curve. In this graph, the overall energy cost savings are visible. The savings result from the decreased overall power consumption, which decreased from 6.76 kWh to 6.44 kWh, as well as from the increased usage of the lower energy prices.

In the course of the validation experiments, the developed virtual sensors, which were used to estimate the heat demand of the machine tool, were also evaluated. For this purpose for pump 1, the rotational speed and electric load, as well as their volume flow, are recorded. An analysis shows that the volume flow was nearly constant at 1.194 ± 0.005 m^3/h during the experiments, indicating that the pump was operated in a constant operational state. The application of the previously developed linear model yields satisfactory results (prediction: 1.167 ± 0.004 m^3/h), with a normalized mean absolute error of only 2.3%.

A measurement of the volume flow of pump 2 yields that the assumption in Section 4 of a constant volume flow of 0.617 m^3/h was not valid. During the experiments, the

pump assumed a volume flow oscillating around 0.537 ± 0.006 m^3/h instead, leading to a normalized mean absolute error of 14.8%. The development of a virtual volume-flow sensor for pump 2 in analogy to pump 1 would therefore be required for the productive implementation of the results.

The results of pump 1 show that the virtual volume-flow sensor is robust and can be used as a valid alternative to a permanent volume-flow metering device. The advantage of a virtual sensor compared to a permanent physical sensor is the reduced investment cost since only a temporary measurement is needed. However, a portable volume-flow meter is required for that. A disadvantage of virtual sensors is the effort needed to take the temporary measurement in several operational states and develop the data-based model. Furthermore, unknown operating states may not be captured by the virtual sensor, as the results of pump 2 show.

7. Conclusions and Outlook

Our approach for the energy-flexible operation of a machine tool with a cooling-supply system, which we have demonstrated and validated on the realistic use case, is a suitable method for the future flexibilization of production processes. We have thereby come to the following central conclusions:

- We successfully combine a generic energy-flexibility data model with energy-oriented production planning. For this purpose, we have taken the material flow of the production process into account when deriving the EFDM.
- Not only the machine tool was considered as a system boundary for energy-flexible operation but also the associated supply systems. This step is necessary to obtain a realistic EFDM with correct dependencies.
- To realize a holistic approach, we show which assumptions and data are required for a correct calculation of the EFDM. Since data from the machines are needed for the calculation but are not always available as measured values, we have implemented a parameter-estimation method.

It has been shown that the applicability of EFDM to direct optimization to reduce energy consumption is possible. By transferring the calculated energy-flexible energy-optimal machine operation to the use case, scalability to real production systems is ensured, with has benefits in terms of the energy and cost savings realized. The approach was validated on a real production machine with supply systems, and its functionality was proven. In the future, the approach will be transferred to many industrial companies within the framework of the synergy project. This will ensure its application to real applications in the industrial landscape. In addition, the ETA research factory is working on the implementation of several combined energy-flexibility measures, which are to be implemented simultaneously. The successfully realized approach allows one to fill the gaps in the previous research completely or partially.

Similarly, the methods and results demonstrated have limitations and give rise to further avenues of research. On the one hand, the effects of production and material flow, as well as maintenance intervals that limit machine availability, need to be considered in more detail. In addition, approaches need to be investigated to reduce the complexity of EFDM key figure calculation and thus improve its applicability. The optimization algorithms used showed good results, reducing the cost of machine operation. In this respect, the additional improvement potential of both longer optimization horizons and rolling optimization approaches are to be evaluated. The improved accuracy of the boundary conditions thus generated can be assumed to result in additional cost savings. Furthermore, the sensitivity and uncertainty of the analysis of the optimization algorithm could be improved in the results. Further potential for research is offered with respect to the data availability when using the virtual sensors. Here, the heat demand prognosis could be improved by permanently learning prognosis algorithms. Similarly, an increase in the model accuracy of the overall system offers further research potential since the system inertia can be better represented in this way. Furthermore, it has to be investigated to what extent the transfer of the system into the EFDM offers the

possibility to trade the system flexibility for the electricity or flexibility market in order to additionally increase the monetary revenues [42]. In summary, the approach reduces the gap between demand flexibility on the production level by adapting to fluctuating electricity prices and energy-optimal production planning as it is currently often used. Thus, the approach can make an active contribution to the energy transition.

Author Contributions: M.L.: Conceptualization, investigation, methodology, and writing—original draft; B.G.: Methodology, software, investigation, and writing—original draft; G.E.: Investigation, validation, and writing—original draft; B.D.: Investigation, formal analysis, and writing—original draft; M.W.: Supervision, funding acquisition, and writing—review editing. All authors have read and agreed to the published version of the manuscript.

Funding: This research was funded by the German Federal Ministry of Education and Research (BMBF) grant number 03SFK3A0-2.

Institutional Review Board Statement: Not applicable.

Informed Consent Statement: Not applicable.

Data Availability Statement: Not applicable.

Acknowledgments: The authors thankfully acknowledge the financial support of the Kopernikus-Project "SynErgie" by the Federal Ministry of Education and Research of Germany (BMBF) and the project supervision by the project management organisation Projektträger Jülich (PtJ).

Conflicts of Interest: The authors declare no conflict of interest.

References

1. Sauer, A.; Abele, E.; Buhl, H.U. (Eds.) *Energieflexibilität in der Deutschen Industrie: Ergebnisse aus dem Kopernikus-Projekt—Snchronisierte und Energieadaptive Produktionstechnik zur Flexiblen Ausrichtung von Industrieprozessen auf eine Fluktuierende ENERGIEVERSORGUNG (SynErgie)*; Fraunhofer: Stuttgart, Germany, 2019.
2. Rogelj, J.; den Elzen, M.; Höhne, N.; Fransen, T.; Fekete, H.; Winkler, H.; Schaeffer, R.; Sha, F.; Riahi, K.; Meinshausen, M. Paris Agreement climate proposals need a boost to keep warming well below 2 °C. *Nature* **2016**, *534*, 631–639. [CrossRef] [PubMed]
3. Bank, L.; Wenninger, S.; Köberlein, J.; Lindner, M.; Kaymakci, C.; Weigold, M.; Sauer, A.; Schilp, J. Integrating Energy Flexibility in Production Planning and Control—An Energy Flexibility Data Model-Based Approach. In Proceedings of the Conference on Production Systems and Logistics: CPSL 2021, Virtual Event, 10–11 August 2021. [CrossRef]
4. Zhang, Q.; Grossmann, I.E. Enterprise-wide optimization for industrial demand side management: Fundamentals, advances, and perspectives. *Chem. Eng. Res. Des.* **2016**, *116*, 114–131. [CrossRef]
5. Wilke, S. Stromverbrauch. 2013. Available online: https://www.umweltbundesamt.de/daten/energie/stromverbrauch (accessed on 23 March 2023).
6. Schott, P.; Sedlmeir, J.; Strobel, N.; Weber, T.; Fridgen, G.; Abele, E. A Generic Data Model for Describing Flexibility in Power Markets. *Energies* **2019**, *12*, 1893. [CrossRef]
7. Pellinger, C.; Schmid, T. *Merit Order der Energiespeicherung 2030: Technoökonomische Analyse Funktionaler Energiespeicher*; FFE: Munich, Germany, 2016.
8. Umweltbundesamt. Potentiale regelbaren Lasten in einem Energieversorgungssystem mit wachsendem Anteil erneuerbarer Energien: FKZ: 3711 97 102. *Clim. Chang.* **2015**. Available online: http://www.umweltbundesamt.de/publikationen/potentiale-regelbarer-lasten-in-einem (accessed on 15 September 2021).
9. Seitz, P.; Abele, E.; Bank, L.; Bauernhansl, T.; Colangelo, E.; Fridgen, G.; Schilp, J.; Schott, P.; Sedlmeir, J.; Strobel, N.; et al. IT-based Architecture for Power Market Oriented Optimization at Multiple Levels in Production Processes. *Procedia CIRP* **2019**, *81*, 618–623. [CrossRef]
10. Roth, S.; Stumpe, L.; Schmiegel, B.; Braunreuther, S.; Schilp, J. An optimization-based approach for the planning of energy flexible production processes with integrated energy storage scheduling. *Procedia CIRP* **2020**, *88*, 258–264. [CrossRef]
11. Kehne, S.; Fimmers, C.; Grundel, L.; Zender, F.; Epple, A.; Storms, S.; Brecher, C. Look-Ahead to Minimize Energy Costs of CNC Milling Machines for a Volatile Energy Price. In Proceedings of the IECON 2019—45th Annual Conference of the IEEE Industrial Electronics Society, Lisbon, Portugal, 14–17 October 2019; pp. 436–441. [CrossRef]
12. Popp, R.S.H.; Liebl, C.; Zaeh, M.F. Evaluation of the energy-flexible operation of machine tool components. *Procedia CIRP* **2017**, *63*, 76–81. [CrossRef]
13. Bahmani, R.; van Stiphoudt, C.; Menci, S.P.; Schöpf, M.; Fridgen, G. Optimal Industrial Flexibility Scheduling Based on Generic Data Format. *Energy Inform.* **2022**, *5*, 26. [CrossRef]
14. Reinhart, G.; Bank, L.; Brugger, M.; Hieronymus, A.; Koberlein, J.; Roth, S.; Bauernhansl, T.; Sauer, A.; Bauer, D.; Kaymakci, C.; et al. *Konzept der Energiesynchronisationsplattform. Diskussionspapier V3*; Beyreuth University: Beyreuth, Germany, 2020.

15. Verein Deutscher Ingenieure e.V. *VDI 5207 Energieflexible Fabrik: Blatt 1*; VDI: Dusseldorf, Germany, 2020.
16. Dickmann, P. (Ed.) *Schlanker Materialfluss: Mit Lean Production, Kanban und Innovationen*, 3rd ed.; VDI-Buch, Springer Vieweg: Berlin/Heidelberg, Germany, 2015. [CrossRef]
17. Pinedo, M.L. *Scheduling*; Springer International Publishing: Cham, Switzerland, 2016. [CrossRef]
18. IntelliDynamics. *Virtual Sensors*; IntelliDynamics: Seattle, WA, USA, 2018.
19. Omega Engineering Inc. *Paddlewheel Flow Meters—Sensors and Sensing Equipment*; Omega Engineering Inc.: Norwalk, CT, USA, 2019.
20. Omega Engineering Inc. *Ultrasonic Flow Meters—Sensors and Sensing Equipment*; Omega Engineering Inc.: Norwalk, CT, USA, 2019.
21. Posselt, G. *Towards Energy Transparent Factories*, 1st ed.; Sustainable Production, Life Cycle Engineering and Management; Springer: Cham, Switzerland, 2016. [CrossRef]
22. Flick, D.; Kuschicke, F.; Schweikert, M.; Thiele, T.; Panten, N.; Thiede, S.; Herrmann, C. Ascertainment of Energy Consumption Information in the Age of Industrial Big Data. *Procedia CIRP* **2018**, *72*, 202–208. [CrossRef]
23. Abele, E.; Beck, M. *Gemeinsamer Schlussbericht zum Projekt ETA-Fabrik: Energieeffiziente Fabrik für Interdisziplinäre Technologie- und Anwendungsforschung*; Technische Universität Darmstadt: Darmstadt, Germany, 2019. [CrossRef]
24. Grundfos GmbH. *Grundfos Magna3*; Grundfos GmbH: Bjerringbro, Denmark, 2021.
25. FLEXIM GmbH. FLUXUS F601 Energy. Available online: https://www.flexim.com/en/products/thermal-energy-meters/fluxus-f601-energy (accessed on 3 March 2021).
26. Stephan, P. *Thermodynamik: Grundlagen und technische Anwendungen Band 1: Einstoffsysteme*, 19., ergänzte aufl. 2013 ed.; Springer Vieweg: Berlin/Heidelberg, Germany, 2013.
27. KSB Aktiengesellschaft. *Pumpenregelung Anlagenautomation*; KSB Aktiengesellschaft: Frankenthal, Germany, 2013.
28. ETA—Energy Technologies and Applications in Production. EMAG VLC 100GT. 2020. Available online: https://eta-fabrik.de/wp-content/uploads/2020/12/ETA_Broschuere_web_deutsch.pdf (accessed on 24 February 2021).
29. ETA—Energy Technologies and Applications in Production. Rittal Blue e+ Chiller. 2020. Available online: https://eta-fabrik.de/ueber-uns/ausstattung/rittal-blue-e-chiller/ (accessed on 24 February 2021).
30. Viessmann Werke GmbH & Co. KG. *Vitocell 100-E SVPA 950 l*; Viessmann Werke GmbH & Co. KG: Allendorf, Germany, 2021.
31. Dietrich, B.; Walther, J.; Weigold, M.; Abele, E. Machine learning based very short term load forecasting of machine tools. *Appl. Energy* **2020**, *276*, 115440. [CrossRef]
32. Baumann, S.; Gnisia, M.; Feifel, U.; Klingauf, U. Identifikation und Behandlung von Ausreißern in Flugbetriebsdaten für Machine Learning Modelle. In *Deutsche Gesellschaft für Luft-und Raumfahrt—Lilienthal-Oberth eV*; Deutsche Gesellschaft fur Luft- und Raumfahrt: Bonn, Germany, 2018.
33. Goodfellow, I.; Bengio, Y.; Courville, A. *Deep Learning*; Adaptive Computation and Machine Learning; The MIT Press: Cambridge, MA, USA, 2016.
34. Bergstra, J.; Yamins, D.; Cox, D. Making a Science of Model Search: Hyperparameter Optimization in Hundreds of Dimensions for Vision Architectures. In Proceedings of the International Conference on Machine Learning, Atlanta, GA, USA, 16–21 June 2013; pp. 115–123.
35. Géron, A. *Hands-On Machine Learning with Scikit-Learn and TensorFlow: Concepts, Tools, and Techniques to Build Intelligent Systems*; O'Reilly Media, UK Ltd.: Farnham, UK, 2017.
36. Pedregosa, F.; Varoquaux, G.; Gramfort, A.; Michel, V.; Thirion, B.; Grisel, O.; Blondel, M.; Prettenhofer, P.; Weiss, R.; Dubourg, V.; et al. Scikit-learn: Machine learning in Python. *J. Mach. Learn. Res.* **2011**, *12*, 2825–2830.
37. Trane Klima- und Kältetechnisches Büro GmbH. *Grundwissen/Grundlagen*; Trane Klima- und Kältetechnisches Büro GmbH: Krailling, Germany, 2021.
38. Kurzweil, P.; Frenzel, B.; Gebhard, F. *Physik Formelsammlung: Für Ingenieure und Naturwissenschaftler*, 1st ed.; Studium Technik; Vieweg: Wiesbaden, Germany, 2008. [CrossRef]
39. Viessmann Werke GmbH & Co. KG. *VITOCELL 300-B: Datenblatt*; Viessmann Werke GmbH & Co. KG: Allendorf, Germany, 2020.
40. IBM. *IBM Documentation*; IBM: Armonk, NY, USA. Available online: https://www.ibm.com/docs/en/www.ibm.com/docs/en/icos (accessed on 2 May 2023).
41. Biel, K.; Glock, C.H. Systematic Literature Review of Decision Support Models for Energy-Efficient Production Planning. *Comput. Ind. Eng.* **2016**, *101*, 243–259. [CrossRef]
42. Lindner, M.; Wenninger, S.; Fridgen, G.; Weigold, M. Aggregating Energy Flexibility for Demand-Side Management in Manufacturing Companies—A Two-Step Method. In *Production at the Leading Edge of Technology*; Behrens, B.A., Brosius, A., Drossel, W.G., Hintze, W., Ihlenfeldt, S., Nyhuis, P., Eds.; Springer eBook Collection; Springer International Publishing and Imprint Springer: Cham, Switzerland, 2022; pp. 631–638. [CrossRef]